

Adaptive Identification of Blurred Regions for Accurate Image Deblurring

Hu Gao
 Beijing Normal University
 Beijing, China
 gao_h@mail.bnu.edu.cn

Depeng Dang
 Beijing Normal University
 Beijing, China
 ddepeng@bnu.edu.cn

Abstract

Image deblurring aims to restore high-quality images from blurred ones. While existing deblurring methods have made significant progress, most overlook the fact that the degradation degree varies across different regions. In this paper, we propose AIBNet, a network that adaptively identifies the blurred regions, enabling differential restoration of these regions. Specifically, we design a spatial feature differential handling block (SFDHBlock), with the core being the spatial domain feature enhancement module (SFEM). Through the feature difference operation, SFEM not only helps the model focus on the key information in the blurred regions but also eliminates the interference of implicit noise. Additionally, based on the fact that the difference between sharp and blurred images primarily lies in the high-frequency components, we propose a high-frequency feature selection block (HFSBlock). The HFSBlock first uses learnable filters to extract high-frequency features and then selectively retains the most important ones. To fully leverage the decoder's potential, we use a pre-trained model as the encoder and incorporate the above modules only in the decoder. Finally, to alleviate the resource burden during training, we introduce a progressive training strategy. Extensive experiments demonstrate that our AIBNet achieves superior performance in image deblurring.

1. Introduction

Image deblurring aims to remove blur and restore clean images. Due to the ill-posed nature of the problem, traditional methods [15] try to tackle it by introducing priors to constrain the solution space. However, formulating these priors is difficult and often lacks broad applicability, making them unsuitable for real-world scenarios.

With the rapid advancement of deep learning, convolutional neural networks (CNNs) [3, 7, 25, 31] have become the preferred approach for image deblurring. They excel at implicitly learning generalized priors by capturing natural image statistics, achieving state-of-the-art performance.



Figure 1. Varying degrees of degradation across different regions. (a) is the blurred image, (b) is the corresponding clear image, and (c) is the residual image between the blurred and clear images.

However, while convolutional operations are effective at modeling local connections, their limited receptive field and inability to adapt to input content restrict the model's ability to capture long-range dependencies. To overcome these limitations, Transformers [8, 10, 20, 28, 40] have been incorporated into image deblurring. With their self-attention mechanism and adaptive weights, Transformers capture global dependencies more effectively, outperforming CNN-based methods. More recently, Mamba-based networks [11, 14, 23] have been applied to image deblurring tasks. These networks capture global information with linear complexity, offering greater efficiency than Transformers.

Although the methods mentioned above have achieved excellent performance through modular design, most overlook the fact that **the degradation degrees varies across different regions of the blurred image**. Treating all regions as having the same degree of degradation inevitably leads to the introduction of artificial artifacts in the restored image. For two examples shown in Figure 1, (a) is the blurred image, (b) is the corresponding clear image, and (c) is the residual image between the blurred and clear images. It is evident that the areas marked with **red boxes** are more heavily degraded, while those marked with **green boxes** exhibit less degradation. The residual images also highlight that the difference between the clear and blurred

image pairs is nearly zero in the less degraded regions. To enable differential handling of varying degrees of degradation, AdaRevD [25] introduces a classifier to assess the degradation degree of image patches. However, this method categorizes patches into six degradation levels based on the PSNR between the blurred and clear patches, and uses a fixed, relatively large patch size of 384 x 384 for classification. This rigid approach reduces its effectiveness in adaptively managing degradation across patches of different sizes.

Based on the above analysis, we are motivated to find a method that can adaptively handle regions with varying degrees of degradation. To achieve this, we propose AIBNet, a network that adaptively identifies blurred regions in both the spatial and frequency domains. Specifically, we design a spatial feature differential handling block (SFDHBlock), consisting of a spatial feature enhancement module (SFEM) and a simple channel attention (SCA) [3]. Drawing from the theory of differential amplifiers, SFEM uses feature differences to remove features from non-blurred regions and reduce implicit noise caused by intensive calculations, helping the model focus on key information in the blurred regions. Meanwhile, we use the SCA to capture spatial domain features. The features from SFEM and SCA are fused using learnable weights, enhancing the representation of features in the blurred regions.

Additionally, recognizing that the difference between clear/blurred images primarily lies in the high-frequency components, we present a high-frequency feature selection block (HFSBlock). The HFSBlock first uses learnable filters to extract high-frequency features, then selectively retains the most important high-frequency information to emphasize the features of the degraded regions. To fully leverage the potential of the decoder, we use a pre-trained model as the encoder and adopt multiple sub-decoders. Finally, to reduce the resource burden during training, we introduce a progressive training strategy.

The main contributions of this work are:

1. We propose an adaptively identifies blurred regions network (AIBNet) for image deblurring. Extensive experiments demonstrate that the proposed AIDNet achieves promising performance across synthetic and real-world datasets.
2. We design a spatial feature differential handling block (SFDHBlock), with the core being the spatial feature enhancement module (SFEM). SFEM uses feature differences to help the model focus on key information in the blurred regions.
3. We present a high-frequency feature selection block (HFSBlock) that extract high-frequency features through learnable filters, and selectively retains the most important high-frequency information.
4. We introduce a progressive training strategy to minimize GPU memory usage during training.

GPU memory usage during training.

2. Related Work

2.1. Traditional methods.

Due to the ill-posed nature of image deblurring, traditional methods [2, 15, 37] primarily rely on hand-crafted priors to constrain the possible solutions. Recently, camera data from inertial measurement units has been leveraged to describe degradation parameters, providing guidance for blur kernel estimation [32]. While these priors can aid in blur removal, they often fail to accurately model the degradation process and lack generalizability.

2.2. CNN-based methods.

With the rapid progress of deep learning, many methods [1, 13, 27] use deep CNNs to address image deblurring, eliminating the need for manually designed image priors. To better balance spatial details and contextual information, MPRNet [39] introduces cross-stage feature fusion to leverage features from multiple stages. IRNeXt [5] rethinks convolutional network design, offering an efficient CNN-based architecture for image restoration. NAFNet [3] evaluates baseline modules and suggests replacing nonlinear activation functions with multiplication, which simplifies the system’s complexity. TURTLE [12] employs a truncated causal history model for efficient, high-performance video restoration. CGNet [13] integrates a global context extractor to effectively capture global information. FSNet [7] uses multi-branch and content-aware modules to dynamically select the most relevant components. ELEDNet [16] leverages cross-modal feature information with a low-pass filter to reduce noise while preserving structural details. MR-VNet [31] utilizes Volterra layers for efficient deblurring. While these methods are superior to traditional methods, the inherent limitations of convolutional operations hinder the models’ ability to effectively capture long-range dependencies.

2.3. Transformer-based methods.

The transformer architecture [35] has gained significant popularity in image deblurring [29, 34, 41, 42] due to its content-dependent global receptive field, showing superior performance over traditional CNN-based baselines. However, image deblurring often deals with high-resolution images, and the attention mechanism in Transformers incurs quadratic time complexity, resulting in significant computational overhead. In order to reduce the computational cost, Uformer [36], SwinIR [21] and U²former [10] computes self-attention based on a window. Restormer [40], MRLPFNet [8], and DeblurDiNAT [22] compute self-attention across channels rather than in the spatial dimension, achieving linear complexity in relation to input size.

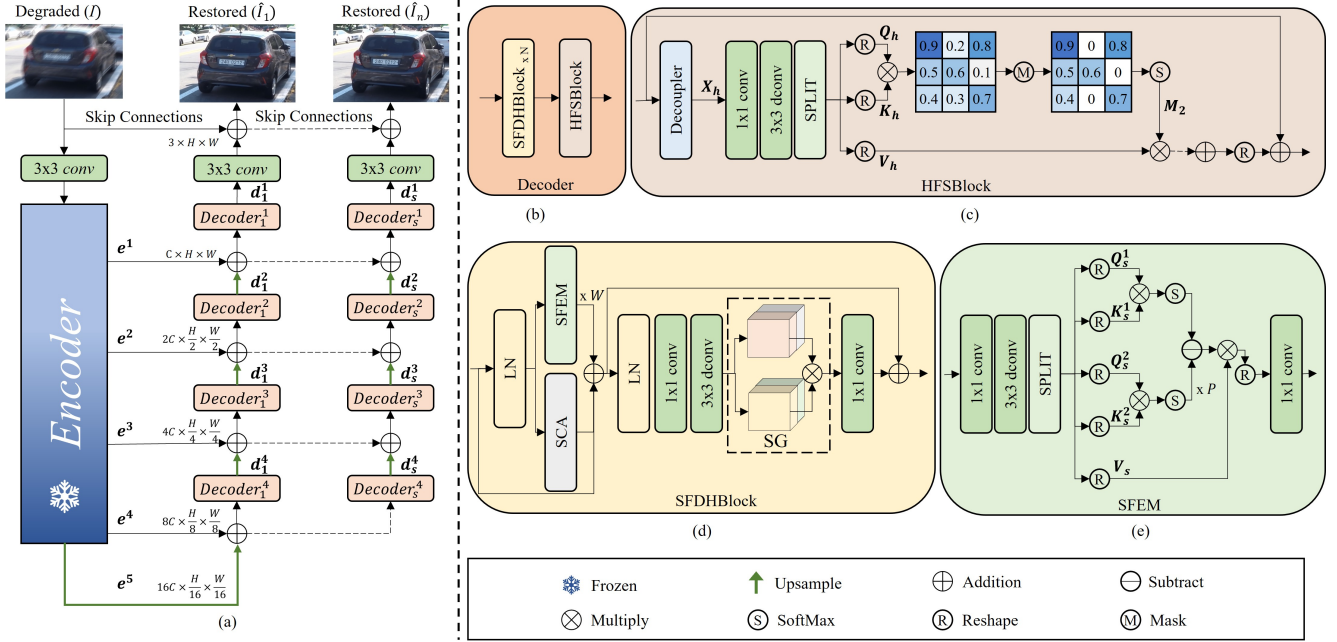


Figure 2. (a) The overall architecture of the proposed AIBNet. (b) The decoder, consisting of N spatial feature differential handling blocks (SFDHBlocks) and a high-frequency feature selection block (HFSBlock). (c) The structure of the HFSBlock is shown, with the case of using a single mask matrix for simplicity. (d) The SFDHBlock, which consists of two branches: the SCA proposed in NAFNet [3] and the spatial feature enhancement module (SFEM). (e) The structure of the SFEM.

However, the above methods inevitably cause feature loss. To this end, FFTformer [18] explores the property of the frequency domain to estimate the scaled dot-product attention. For realistic image deblurring, HI-Diff [4] harnesses the power of diffusion models to generate informative priors, which are then integrated hierarchically into the deblurring process to improve results.

Although the methods mentioned above have achieved excellent performance through modular design, most overlook the fact that the degradation degrees varies across different regions of the blurred image. To enable differential processing of varying degrees of degradation, AdaRevD [25] introduces a classifier to assess the degradation degree of image patches, but it relies on a limited number of predefined categories and a fixed patch size. This rigid approach reduces its effectiveness in adaptively managing degradation across patches of different sizes. In this paper, we propose an adaptively identifies blurred regions network for image deblurring, named AIBNet, which adept at differential handle regions with varying degrees of degradation

3. Method

In this section, we first provide an overview of the entire AIBNet pipeline. We then dive into the details of the proposed decoder, which comprises two main components:

the spatial feature differential handling block (SFDHBlock) and the high-frequency feature selection block (HFSBlock). Lastly, we present the progressive training strategy.

3.1. Overall Pipeline

Our proposed AIBNet, as shown in Figure 2 (a), includes a frozen encoder and s sub-decoders. Each sub-decoder consists of N SFDHBlocks and a HFSBlock. Given a degraded image $\mathbf{I} \in \mathbb{R}^{H \times W \times 3}$, AIBNet first uses a convolutional layer to extract shallow features $\mathbf{F} \in \mathbb{R}^{H \times W \times C}$, where H , W , and C represent the height, width, and number of channels of the feature map, respectively. These shallow features are passed through a pre-trained encoder to produce encoder features e^i (where $i = 1, 2, 3, 4, 5$) at different scales. The encoder features are then fed into the decoder, which generates decoder features d_s^i at different scales, progressively restoring them to their original size. It is important to note that, since our model includes multiple sub-decoders, the input to each subsequent sub-decoder is the output of the previous one. Finally, convolution is applied to the refined features to produce the residual image $\mathbf{X}_s \in \mathbb{R}^{H \times W \times 3}$ for s^{th} sub-decoder. This residual image is added to the degraded image to produce the restored output: $\hat{\mathbf{I}}_s = \mathbf{X}_s + \mathbf{I}$.

3.2. Spatial Feature Differential Handling Block

Most previous image deblurring methods achieve excellent performance by designing novel modules, but they often

overlook the fact that the blur degree varies across different regions. To address this issue, we first design a spatial domain feature differential handling block (SFDHBlock), which helps the model focus on the key information of the blurred regions by removing the features of the non-blurred regions. As shown in Figure 2(d), given the input features at the $(l-1)$ th block X_{l-1} , the procedures of SFDHBlock can be defined as:

$$\begin{aligned} X_{l-1}^n &= LN(X_{l-1}) \\ X_l' &= X_{l-1} + SCA(X_{l-1}') + W \cdot SFEM(X_{l-1}^n) \quad (1) \\ X_l &= X_l' + f_{1 \times 1}^c(SG(f_{3 \times 3}^{dwc}(f_{1 \times 1}^c(LN(X_l'))))) \end{aligned}$$

where LN denotes Layer Normalization, $f_{3 \times 3}^{dwc}$ refers to the 3×3 depth-wise convolution, and $f_{1 \times 1}^c$ represents the 1×1 convolution. W is the learnable parameter, which is directly optimized through backpropagation and initialized to 1. It's worth noting that our design is highly lightweight, as it does not introduce additional convolution layers. SCA stands for Simple Channel Attention, as proposed in NAFNet [3]. SFEM represents the spatial feature enhancement module, which is described below.

3.2.1. Spatial Feature Enhancement Module

Inspired by the theory of differential amplifiers, where the difference between two signals cancels out common-mode noise, we design the spatial feature enhancement module (SFEM). SFEM leverages feature differences to remove features from non-blurred regions and reduce implicit noise caused by intensive calculations, thereby helping the model focus on the key information in the blurred regions. As shown in Figure 2(c), we first encode channel-wise context by applying 1×1 convolutions followed by 3×3 depth-wise convolutions. Next, the feature is divided into five parts and reshaped to enable the subsequent attention calculation in the channel dimension, thereby reducing both time and memory complexity. Among these five features, we partition the query and key vectors into two groups and compute two separate *SoftMax* attention maps. The result of subtracting these two maps is then used as the attention scores. Formally, given the features X_{l-1}^n after LN, we can obtain the enhanced features X_{l-1}^e by the following:

$$\begin{aligned} X_{l-1}^c &= f_{3 \times 3}^{dwc}(f_{1 \times 1}^c(X_{l-1}^n)) \\ Q_s^1, K_s^1, Q_s^2, K_s^2, V_s &= SPLIT(X_{l-1}^c) \\ att1 &= SoftMax\left(\frac{Q_s^1 T(K_s^1)}{\beta}\right) \quad (2) \\ att2 &= SoftMax\left(\frac{Q_s^2 T(K_s^2)}{\beta}\right) \\ X_{l-1}^e &= f_{1 \times 1}^c(Reshape((att1 - \alpha \cdot att2)V_s)) \end{aligned}$$

β is a learning scaling parameter used to adjust the magnitude of the dot product before applying the *SoftMax*

function, and it is initialized as $\beta = \sqrt{C}$. T denotes the transpose operation. α is the learnable scalar, initialized as:

$$\alpha = \exp(\alpha_{Q_s^1} \cdot \alpha_{K_s^1}) - \exp(\alpha_{Q_s^2} \cdot \alpha_{K_s^2}) + \alpha_{init} \quad (3)$$

where $\alpha_{Q_s^1}, \alpha_{K_s^1}, \alpha_{Q_s^2}, \alpha_{K_s^2}$ are the learnable parameters, which are directly optimized through backpropagation. And α_{init} a constant used for the initialization.

Finally, as shown in Eq. 1, the enhanced feature $X_{l-1}^e = SFEM(X_{l-1}^n)$ is fused with the other branches. This offers several advantages. First, SFEM addresses the limitation of SCA in modeling long-range dependencies. Second, SFEM enhances the features of blurred regions, making it easier for the model to focus on the most relevant information and achieve better restoration performance. Lastly, SFEM reduces the impact of implicit noise caused by intensive calculations through feature differences.

3.3. High-frequency Feature Selection Block

Based on the theory that the difference between blurred and sharp image pairs primarily lies in the high-frequency components [5], we design the high-frequency feature selection block (HFSBlock) to further refine the identification of blurred regions in the frequency domain. The key motivation of our HFSBlock is to perform differential handling of different blurred regions. To achieve this, we do not design a new high-frequency feature capture module; instead, we use the existing Decoupler [7] to dynamically generate high-frequency features X_h . These high-frequency features are then aggregated to leverage the sparsity by dynamically masking irrelevant features, thereby selecting the most important high-frequency components to retain for identifying blurred regions. For simplicity, we only show the case of using a single mask matrix in Figure 2(c). Specifically, given the output features X_N of the N th SFDHBlock, we first dynamically generate the high-frequency features X_h as follows:

$$X_h = Decoupler(X_N) \quad (4)$$

Similar to SFEM, we apply 1×1 and 3×3 convolutions, followed by splitting and reshaping, to obtain the query Q_h , key K_h , and value V_h matrices with the shape of $C \times H \times W$. Next, a dense attention matrix of shape $C \times C$ is generated by performing a dot-product operation between Q_h and transposed K_h across channels. Then, we selectively mask out the irrelevant elements to retain the most important high-frequency components for identifying blurred regions in the dense attention matrix. In the example shown in Figure 2(c), we obtain the sparse attention matrix M_2 by keeping the first $\frac{2}{3}$ of the elements and setting the rest to 0 through masking. To maintain flexibility, we pass n_m mask matrices and *SoftMax* to obtain n_m sparse attention matrices M_i ($i = 1, 2, 3, \dots, n_m$), and then perform a dot-product operation with V_h , respectively. Finally, the

results are fused using learnable parameters and reshape to the original size to get the selection high-frequency features X_{sh} . The specific process is as follows:

$$M_i = \text{SoftMax}(\text{Mask}_i(\frac{Q_h T(K_h)}{\beta})) \quad (5)$$

$$X_{sh} = X_N + \text{Reshape}(\sum_{i=1}^{n_m} \lambda_i M_i \times V)$$

where λ_i denotes the learnable parameters to control the dynamic selection of fusion. Mask_i is the i_{th} mask matrices, which defined as:

$$\text{Mask}_i(x) = \begin{cases} x, x \in \text{fist} \frac{i}{i+1}, \\ 0, \text{otherwise.} \end{cases} \quad (6)$$

Since feature difference has already been applied in SFEM, the high-frequency feature values with large responses in HFSBlock do not contain implicit noise. Therefore, HFSBlock retains the values of elements that align with the response and simply sets the elements that do not match the response to 0. This ensures the accuracy of the high-frequency features. The feature representation of blurred regions is enhanced both in the spatial domain by SFEM and in the frequency domain by HFSBlock, enabling our model to adaptively identify blurred regions for differential processing and accurate image deblurring.

3.4. Progressive Training Strategy

Since our model contains multiple sub-decoders, training it directly can be highly demanding on GPU memory. Additionally, to simplify the model and reduce computational complexity, we avoid introducing complex discriminative fusion mechanisms to connect the features of each sub-decoder. However, since the input of each subsequent sub-decoder depends heavily on the output of the previous one, the absence of such mechanisms can lead to issues like gradient collapse. To address this, we propose a progressive training strategy, where only one sub-decoder is trained at a time. After each sub-decoder is trained, its parameters are frozen before training the next one. This strategy offers multiple advantages. First, by training only one sub-decoder at a time, we significantly reduce the GPU memory requirements. Second, because each sub-decoder is trained with the actual image data, the input features for the next sub-decoder are more accurate, leading to better performance.

To optimize the proposed network AIBNet by minimiz-

ing the following loss function:

$$L = L_c(\hat{I}_s, \bar{I}) + \delta L_e(\hat{I}_s, \bar{I}) + \lambda L_f(\hat{I}_s, \bar{I}) \quad (7)$$

$$L_c = \sqrt{\|\hat{I}_s - \bar{I}\|^2 + \epsilon^2}$$

$$L_e = \sqrt{\|\Delta \hat{I}_s - \Delta \bar{I}\|^2 + \epsilon^2}$$

$$L_f = \|\mathcal{F}(\hat{I}_s) - \mathcal{F}(\bar{I})\|_1$$

where \bar{I} denotes the target image and \hat{I}_s represents the output of the s_{th} sub-decoder. L_c refers to the Charbonnier loss with a constant of $\epsilon = 0.001$, while L_e is the edge loss, where Δ denotes the Laplacian operator. L_f represents the frequency domain loss, with \mathcal{F} indicating the fast Fourier transform. To balance the contributions of the loss terms, we set the parameters $\lambda = 0.1$ and $\delta = 0.05$, as in [7, 39].

4. Experiments

In this section, we detail the experimental setup and provide both qualitative and quantitative comparisons. We also conduct ablation studies to demonstrate the effectiveness of our approach. The best and second-best results in the tables are highlighted in **bold** and underlined, respectively.

4.1. Experimental Settings

4.1.1. Training details

We use the Adam optimizer [17] with parameters $\beta_1 = 0.9$ and $\beta_2 = 0.999$. The initial learning rate is set to 2×10^{-4} and is gradually reduced to 1×10^{-7} using the cosine annealing strategy [24]. The networks are trained on 256×256 patches with a batch size of 32 for 4×10^5 iterations. Data augmentation includes both horizontal and vertical flips. For each decoder, we set N (see Figure 2(b)) to 8. Additionally, we build 3 versions of AIBNet by varying the number of sub-decoders s (see Figure 2(a)): AIBNet-S (1 sub-decoder), AIBNet-B (2 sub-decoders), and AIBNet-L (4 sub-decoders). For the encoder, we use UFPNet [9].

4.1.2. Datasets

We evaluate the effectiveness of our method using the GoPro dataset [26], which includes 2,103 training image pairs and 1,111 evaluation pairs. To assess the generalizability of our model, we apply the GoPro-trained model to the HIDE [33] dataset, consisting of 2,025 images. Both the GoPro and HIDE datasets are synthetically generated. Additionally, we test our method on real-world images using the RealBlur [30] dataset, which contains 3,758 training image pairs and 980 testing pairs, divided into two subsets: RealBlur-J and RealBlur-R.

4.2. Experimental Results

4.2.1. Evaluations on the synthetic dataset.

Table 1 presents the performance of various image deblurring methods on the synthetic GoPro [26] and HIDE [33]

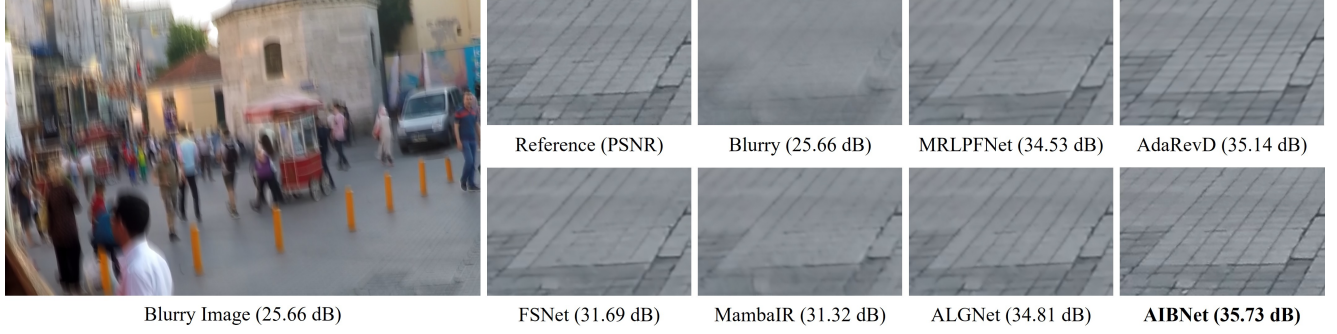


Figure 3. Image deblurring comparisons on the synthetic dataset [26].



Figure 4. Image deblurring comparisons on the real-world dataset [30].

Table 1. Quantitative evaluations of the proposed approach against state-of-the-art motion deblurring methods. Our AIBNet and AIBNet-B are trained only on the GoPro dataset [26].

Methods	GoPro		HIDE	
	PSNR ↑	SSIM ↑	PSNR ↑	SSIM ↑
MPRNet [39]	32.66	0.959	30.96	0.939
Restormer [40]	32.92	0.961	31.22	0.942
Uformer [36]	32.97	0.967	30.83	0.952
NAFNet-64 [3]	33.62	0.967	-	-
IRNeXt [5]	33.16	0.962	-	-
SFNet [6]	33.27	0.963	31.10	0.941
DeepRFT+ [38]	33.23	0.963	31.66	0.946
UFPNet [9]	34.06	0.968	31.74	0.947
MRLPFNet [8]	34.01	0.968	31.63	0.947
MambaIR [14]	33.21	0.962	31.01	0.939
ALGNet [11]	34.05	0.969	31.68	<u>0.952</u>
MR-VNet [31]	34.04	0.969	31.54	0.943
FSNet [7]	33.29	0.963	31.05	0.941
AdaRevD-L [25]	34.60	0.972	<u>32.35</u>	0.953
AIBNet-S(Ours)	34.47	0.971	32.19	0.949
AIBNet-B(Ours)	<u>34.69</u>	<u>0.972</u>	<u>32.35</u>	<u>0.952</u>
AIBNet-L(Ours)	34.95	0.974	32.41	0.953

datasets. Overall, AIBNet outperforms competing methods, delivering higher-quality images with improved PSNR and SSIM values. Specifically, compared to the previous best

method, AdaRevD-L [25], our AIBNet-L achieves a 0.35 dB improvement on the GoPro [26] dataset. Remarkably, even though our model was trained solely on the GoPro [26] dataset, it still achieves state-of-the-art results (32.41 dB in PSNR) on the HIDE [33] dataset, demonstrating its strong generalization ability. Performance further improves as the model size increases (from AIBNet-S to AIBNet-L), emphasizing the scalability of our approach. Finally, Figure 3 showcases deblurred images from different methods, with our model’s outputs being sharper and closer to the ground truth than those of other methods.

4.2.2. Evaluations on the real-world dataset.

We further assess the performance of our AIBNet on real-world images from the RealBlur dataset [30]. As shown in Table 2, our method achieves superior PSNR and SSIM scores. Specifically, compared to the previous best method, AdaRevD-L [25], our approach improves PSNR by 0.25 dB on the RealBlur-R dataset and 0.13 dB on the RealBlur-J dataset. Figure 4 illustrates how our method effectively removes real blur while maintaining structural and textural details. In contrast, images restored by other methods either appear overly smooth or fail to effectively eliminate the blur.

Table 2. Quantitative evaluations of the proposed approach against state-of-the-art methods on the real-word dataset RealBlur [30].

Methods	RealBlur-R		RealBlur-J	
	PSNR \uparrow	SSIM \uparrow	PSNR \uparrow	SSIM \uparrow
DeblurGAN-v2 [19]	36.44	0.935	29.69	0.870
MPRNet [39]	39.31	0.972	31.76	0.922
DeepRFT+ [38]	39.84	0.972	32.19	0.931
Stripformer [34]	39.84	0.975	32.48	0.929
FFTformer [18]	40.11	0.973	32.62	0.932
UFPNet [9]	40.61	0.974	33.35	0.934
MambaIR [14]	39.92	0.972	32.44	0.928
ALGNet [11]	41.16	0.981	32.94	0.946
MR-VNet [31]	40.23	0.977	32.71	0.941
AdaRevD-L [25]	41.19	0.979	33.96	0.944
AIBNet-S(Ours)	41.12	0.980	33.88	0.956
AIBNet-B(Ours)	41.23	0.980	33.97	0.955
AIBNet-L(Ours)	41.44	0.981	34.09	0.958

Table 3. Ablation study on individual components of the proposed AIBNet.

Net	Pre-trained	SFEM	HFSBlock	PSNR	Δ PSNR
(a)				33.62	-
(b)		✓		33.93	+0.31
(c)			✓	33.92	+0.30
(d)		✓	✓	34.32	+0.70
(e)	✓	✓	✓	34.47	+0.85

4.3. Ablation Studies

In this section, we first showcase the effectiveness of the proposed modules and then explore the impact of different design choices for each module. Due to page limits, more experiments are presented in the supplementary material.

4.3.1. Effects of individual components

To assess the impact of each module, we use NAFNet [3] as the baseline and progressively replace or add our proposed modules. As shown in Table 3(a), the baseline achieves a PSNR of 33.62 dB. Each module combination leads to a noticeable performance improvement. Specifically, adding the SFEM to NAFBlock [3] improves performance by 0.31 dB (Table 3(b)). Incorporating the HFSBlock into the original NAFNet [3] results in a significant increase in performance, boosting the PSNR from 33.62 dB to 34.92 dB (Table 3(c)). When both SFEM and HFSBlock are combined (Table 3(d)), our model achieves a 0.70 dB improvement over the original baseline. Finally, using a pre-trained model as the encoder and training only the decoder leads to a performance of 34.47 dB.

To further validate the effectiveness of the proposed module, we visualize the feature maps within it. Figure 5 presents a visual comparison. In the initial features, main structures, such as the license plate number in Figure 5(b), are not well recovered before applying SFEM. In contrast,

Table 4. Effect of the number of mask matrices in HFSBlock.

Net	Number	PSNR	Δ PSNR
(a)	0	34.22	-
(b)	1	34.35	+0.13
(c)	2	34.40	+0.18
(d)	3	34.43	+0.21
(e)	4	34.47	+0.25
(f)	5	34.46	+0.24

Table 5. Effect of the pre-trained models.

Net	Pre-trained	Trainable	PSNR	Δ PSNR
	NAFNet [3]	UFPNet [9]		
(a)			34.64	-
(b)	✓	✓	34.79	+0.15
(c)	✓		34.77	+0.13
(e)		✓	34.79	+0.15
(f)		✓	34.81	+0.17

after the application of SFEM, as shown in Figure 5(c), the features are enhanced, allowing for a clearer representation of spatial details and more distinct structures.

In HFSBlock, we selectively retain the most important high-frequency information. To better understand this mechanism, we compare the feature maps with and without HFSBlock in Figure 6. With our high-frequency feature selection, HFSBlock reveals finer details, such as pedestrians and graffiti on walls.

4.3.2. Effect of the number of mask matrices

The core component of HFSBlock is the mask matrix, which identifies the degraded regions by selectively preserving the most crucial high-frequency information and enhancing the frequency difference in those areas. To evaluate the impact of the number of mask matrices on model performance, we present the results in Table 4 for various configurations. As shown in Eq 6, the i_{th} mask matrix retain the elements of the first $\frac{i}{i+1}$ and the others are set to 0. As shown in Table 4 (a), the performance is poorest at 34.22 dB when no mask matrix. However, performance improves as we incorporate different masking strategies with an increased number of mask matrices. Table 4 (e) shows that the best performance is achieved with four mask matrices. Adding more mask matrices beyond this point results in a slight degradation in performance (see Table 4 (f)), as irrelevant or unnecessary feature representations are introduced.

4.3.3. Effects of the pre-trained models

Since our AIBNet utilizes an existing pre-trained model as the encoder, we evaluate the impact of different pre-trained models on performance. As shown in Table 5, the results vary with different pre-trained models (NAFNet [3], UFPNet [9]), but all contribute to the model performance. Addi-



Figure 5. The internal features of the SFEM. With our spatial feature enhancement, the SFEM captures finer details, such as the number plate, compared to the initial features. Zoom in for a clearer view.

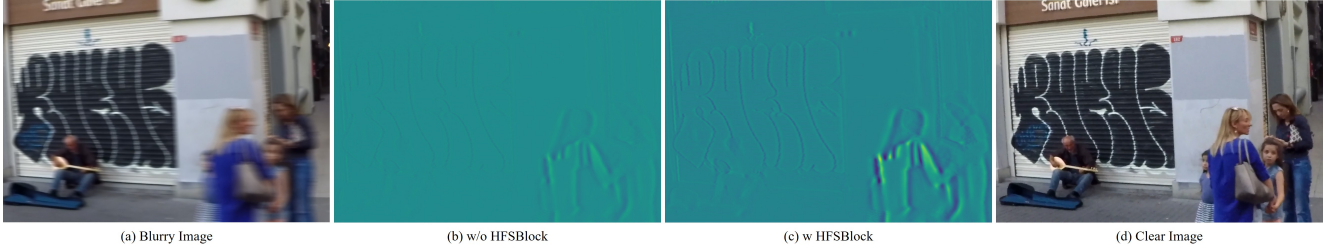


Figure 6. The features of HFSBlock. With our high-frequency feature selection, HFSBlock produces more fine details, such as pedestrians and graffiti on walls.

Table 6. Effect of the progressive training strategy, where $\#P$ denotes the parameters.

Net	Fusion	Progressive	PSNR	Δ PSNR	Δ $\#P(M)$
(a)			34.68	-	-
(b)	SAM [39]		34.72	+0.04	+6.12
(c)	Fuse [25]		34.71	+0.03	+1.32
(d)		✓	34.81	+0.13	-122.01

tionally, we examine how freezing the encoder parameters affects performance. From Table 5 (b) and (c), we observe that when NAFNet is used as the pre-trained model, freezing the encoder parameters leads to a decrease in performance. However, when UFPNet is used as the pre-trained model, freezing the parameters improves performance (see Table 5 (e) and (f)). Overall, freezing the encoder parameters has a minimal impact on performance. To save computational resources, we opt to freeze the encoder parameters and only train the decoder.

4.3.4. Effects of the progressive training strategy

As shown in Table 6(a), the worst performance occurs when multiple sub-decoders are trained directly. Adding a fusion module between the sub-decoders (Table 6(b) and (c)) improves performance, but also introduces additional parameters. When the progressive training strategy is applied (Table 6(d)), the performance is optimized. Moreover, since only one sub-decoder is trained at a time, our strategy is resource-efficient. Compared to direct training, the number of trainable parameters is drastically reduced by 122.01M.

Table 7. The evaluation of model computational complexity.

Method	Time(s)	MACs(G)	PSNR↑	SSIM↑
MPRNet	1.148	777	32.66	0.959
MambaIR [14]	0.743	439	33.21	0.962
AdaRevD-L [25]	0.761	460	34.60	<u>0.972</u>
AIBNet-S(Ours)	0.241	114	34.47	0.971
AIBNet-B(Ours)	<u>0.552</u>	<u>228</u>	<u>34.69</u>	<u>0.972</u>
AIBNet-L(Ours)	0.729	456	34.95	0.974

4.4. Resource Efficient

We evaluate the model complexity of our proposed approach and other state-of-the-art methods in terms of running time and MACs. As shown in Table 7, our method achieves the lowest MACs value while delivering competitive performance in terms of running time. However, due to the inclusion of multiple sub-decoders, the complexity of our system is relatively high, reaching 114G MACs. Nonetheless, by leveraging the progressive training strategy introduced in this paper, the training process remains resource-efficient, requiring less computational power.

5. Conclusion

In this paper, we propose an adaptively identifies blurred regions network (AIBNet) for image deblurring. Specifically, we design a spatial feature differential handling block (SFDHBlock) with the core being the spatial feature enhancement module (SFEM), which uses feature differences to help the model focus on key informa-

tion. Additionally, we present a high-frequency feature selection block (HFSBlock), which uses learnable filters to extract and selectively retain the most important high-frequency features. To fully leverage the decoder’s potential, we use a pre-trained model as the encoder and apply the above modules in the decoder. Finally, to reduce the resource burden during training, we employ a progressive training strategy. Extensive experiments show that AIBNet achieves superior performance.

References

- [1] Dongdong Chen and Mike E Davies. Deep decomposition learning for inverse imaging problems. In *Proceedings of the European Conference on Computer Vision (ECCV)*, 2020. 2
- [2] Liang Chen, Faming Fang, Shen Lei, Fang Li, and Guixu Zhang. Enhanced sparse model for blind deblurring. In *Proceedings of the European Conference on Computer Vision*, page 631–646, 2020. 2
- [3] Liangyu Chen, Xiaojie Chu, Xiangyu Zhang, and Jian Sun. Simple baselines for image restoration. *ECCV*, 2022. 1, 2, 3, 4, 6, 7
- [4] Zheng Chen, Yulun Zhang, Ding Liu, bin xia, Jinjin Gu, Linghe Kong, and Xin Yuan. Hierarchical integration diffusion model for realistic image deblurring. In *Proceedings of the Advances in Neural Information Processing Systems*, pages 29114–29125, 2023. 3
- [5] Yuning Cui, Wenqi Ren, Sining Yang, Xiaochun Cao, and Alois Knoll. Irnext: Rethinking convolutional network design for image restoration. In *Proceedings of the 40th International Conference on Machine Learning*, 2023. 2, 4, 6
- [6] Yuning Cui, Yi Tao, Zhenshan Bing, Wenqi Ren, Xinwei Gao, Xiaochun Cao, Kai Huang, and Alois Knoll. Selective frequency network for image restoration. In *The Eleventh International Conference on Learning Representations*, 2023. 6
- [7] Yuning Cui, Wenqi Ren, Xiaochun Cao, and Alois Knoll. Image restoration via frequency selection. *IEEE Transactions on Pattern Analysis and Machine Intelligence*, 46(2):1093–1108, 2024. 1, 2, 4, 5, 6
- [8] J. Dong, J. Pan, Z. Yang, and J. Tang. Multi-scale residual low-pass filter network for image deblurring. In *2023 IEEE/CVF International Conference on Computer Vision (ICCV)*, pages 12311–12320, 2023. 1, 2, 6
- [9] Zhenxuan Fang, Fangfang Wu, Weisheng Dong, Xin Li, Jian Wu, and Guangming Shi. Self-supervised non-uniform kernel estimation with flow-based motion prior for blind image deblurring. In *Proceedings of the IEEE/CVF Conference on Computer Vision and Pattern Recognition (CVPR)*, pages 18105–18114, 2023. 5, 6, 7
- [10] Xin Feng, Haobo Ji, Wenjie Pei, Jinxing Li, Guangming Lu, and David Zhang. U2-former: Nested u-shaped transformer for image restoration via multi-view contrastive learning. *IEEE Transactions on Circuits and Systems for Video Technology*, pages 1–1, 2024. 1, 2
- [11] Hu Gao, Bowen Ma, Ying Zhang, Jingfan Yang, Jing Yang, and Depeng Dang. Learning enriched features via selective state spaces model for efficient image deblurring. In *ACM Multimedia 2024*, 2024. 1, 6, 7
- [12] Amirhosein Ghasemabadi, Muhammad Kamran Janjua, Mohammad Salameh, and Di Niu. Learning truncated causal history model for video restoration. In *The Thirty-eighth Annual Conference on Neural Information Processing Systems*, 2024. 2
- [13] Amirhosein Ghasemabadi, Muhammad Kamran Janjua, Mohammad Salameh, CHUNHUA ZHOU, Fengyu Sun, and Di Niu. Cascadedgaze: Efficiency in global context extraction for image restoration. *Transactions on Machine Learning Research*, 2024. 2
- [14] Hang Guo, Jinmin Li, Tao Dai, Zhihao Ouyang, Xudong Ren, and Shu-Tao Xia. Mambair: A simple baseline for image restoration with state-space model. In *Proceedings of the European Conference on Computer Vision (ECCV)*, 2025. 1, 6, 7, 8
- [15] Ali Karaali and Claudio Rosito Jung. Edge-based defocus blur estimation with adaptive scale selection. *IEEE Transactions on Image Processing*, 27(3):1126–1137, 2017. 1, 2
- [16] Taewoo Kim, Jaeseok Jeong, Hoonhee Cho, Yuhwan Jeong, and Kuk-Jin Yoon. Towards real-world event-guided low-light video enhancement and deblurring. In *Proceedings of the European Conference on Computer Vision (ECCV)*, pages 433–451, 2025. 2
- [17] D. Kingma and J. Ba. Adam: A method for stochastic optimization. *Computer Science*, 2014. 5
- [18] Lingshun Kong, Jiangxin Dong, Jianjun Ge, Mingqiang Li, and Jinshan Pan. Efficient frequency domain-based transformers for high-quality image deblurring. In *Proceedings of the IEEE/CVF Conference on Computer Vision and Pattern Recognition*, pages 5886–5895, 2023. 3, 7
- [19] Orest Kupyn, T. Martyniuk, Junru Wu, and Zhangyang Wang. Deblurgan-v2: Deblurring (orders-of-magnitude) faster and better. *2019 IEEE/CVF International Conference on Computer Vision (ICCV)*, pages 8877–8886, 2019. 7
- [20] Miaoyu Li, Ying Fu, Tao Zhang, Ji Liu, Dejing Dou, Chenggang Yan, and Yulun Zhang. Latent diffusion enhanced rectangle transformer for hyperspectral image restoration. *IEEE Transactions on Pattern Analysis and Machine Intelligence*, 47(1):549–564, 2025. 1
- [21] Jingyun Liang, Jie Zhang, Guolei Sun, Kai Zhang, Luc Van Gool, and Radu Timofte. Swinir: Image restoration using swin transformer. *arXiv preprint arXiv:2108.10257*, 2021. 2
- [22] Hanzhou Liu, Binghan Li, Chengkai Liu, and Mi Lu. Deblurdinat: A lightweight and effective transformer for image deblurring, 2024. 2
- [23] Mingyu Liu, Yuning Cui, Wenqi Ren, Juxiang Zhou, and Alois C. Knoll. Liednet: A lightweight network for low-light enhancement and deblurring. *IEEE Transactions on Circuits and Systems for Video Technology*, pages 1–1, 2025. 1
- [24] I. Loshchilov and F. Hutter. Sgdr: Stochastic gradient descent with warm restarts. 2016. 5
- [25] Xintian Mao, Qingli Li, and Yan Wang. Adarevd: Adaptive patch exiting reversible decoder pushes the limit of image deblurring. In *Proceedings of the IEEE/CVF Conference*

on Computer Vision and Pattern Recognition (CVPR), pages 25681–25690, 2024. 1, 2, 3, 6, 7, 8

[26] Seungjun Nah, Tae Hyun Kim, and Kyoung Mu Lee. Deep multi-scale convolutional neural network for dynamic scene deblurring. *2017 IEEE Conference on Computer Vision and Pattern Recognition (CVPR)*, pages 257–265, 2016. 5, 6

[27] Jinshan Pan, Deqing Sun, Jiawei Zhang, Jinhui Tang, Jian Yang, Yu Wing Tai, and Ming Hsuan Yang. Dual convolutional neural networks for low-level vision. *International Journal of Computer Vision*, 2022. 2

[28] Vaishnav Potlapalli, Syed Waqas Zamir, Salman Khan, and Fahad Shahbaz Khan. Promptir: Prompting for all-in-one blind image restoration. *Advances in Neural Information Processing Systems (NeurIPS)*, 2023. 1

[29] Chen Rao, Guangyuan Li, Zehua Lan, Jiakai Sun, Junsheng Luan, Wei Xing, Lei Zhao, Huaizhong Lin, Jianfeng Dong, and Dalong Zhang. Rethinking video deblurring with wavelet-aware dynamic transformer and diffusion model. In *Proceedings of the European Conference on Computer Vision (ECCV)*, page 421–437, 2025. 2

[30] Jaesung Rim, Haeyun Lee, Jucheol Won, and Sunghyun Cho. Real-world blur dataset for learning and benchmarking deblurring algorithms. In *Proceedings of the European Conference on Computer Vision (ECCV)*, 2020. 5, 6, 7

[31] Siddharth Roheda, Amit Unde, and Loay Rashid. Mr-vnet: Media restoration using volterra networks. In *Proceedings of the IEEE/CVF Conference on Computer Vision and Pattern Recognition (CVPR)*, pages 6098–6107, 2024. 1, 2, 6, 7

[32] Jianxiang Rong, Hua Huang, and Jia Li. Imu-assisted accurate blur kernel re-estimation in non-uniform camera shake deblurring. *IEEE Transactions on Image Processing*, 33: 3823–3838, 2024. 2

[33] Ziyi Shen, Wenguan Wang, Xiankai Lu, Jianbing Shen, Haibin Ling, Tingfa Xu, and Ling Shao. Human-aware motion deblurring. *2019 IEEE/CVF International Conference on Computer Vision (ICCV)*, pages 5571–5580, 2019. 5, 6

[34] Fu-Jen Tsai, Yan-Tsung Peng, Yen-Yu Lin, Chung-Chi Tsai, and Chia-Wen Lin. Stripformer: Strip transformer for fast image deblurring. In *ECCV*, 2022. 2, 7

[35] A. Vaswani, N. Shazeer, N. Parmar, J. Uszkoreit, L. Jones, A. N. Gomez, L. Kaiser, and I. Polosukhin. Attention is all you need. *arXiv*, 2017. 2

[36] Zhendong Wang, Xiaodong Cun, Jianmin Bao, Wengang Zhou, Jianzhuang Liu, and Houqiang Li. Uformer: A general u-shaped transformer for image restoration. In *Proceedings of the IEEE/CVF Conference on Computer Vision and Pattern Recognition (CVPR)*, pages 17683–17693, 2022. 2, 6

[37] Fei Wen, Rendong Ying, Yipeng Liu, Peilin Liu, and Trieu-Kien Truong. A simple local minimal intensity prior and an improved algorithm for blind image deblurring. *IEEE Transactions on Circuits and Systems for Video Technology*, 31(8):2923–2937, 2021. 2

[38] Mao Xintian, Liu Yiming, Liu Fengze, Li Qingli, Shen Wei, and Wang Yan. Intriguing findings of frequency selection for image deblurring. In *Proceedings of the 37th AAAI Conference on Artificial Intelligence*, 2023. 6, 7

[39] Syed Waqas Zamir, Aditya Arora, Salman Khan, Munawar Hayat, Fahad Shahbaz Khan, Ming-Hsuan Yang, and Ling Shao. Multi-stage progressive image restoration. In *CVPR*, 2021. 2, 5, 6, 7, 8

[40] Syed Waqas Zamir, Aditya Arora, Salman Khan, Munawar Hayat, Fahad Shahbaz Khan, and Ming-Hsuan Yang. Restormer: Efficient transformer for high-resolution image restoration. In *CVPR*, 2022. 1, 2, 6

[41] Huicong Zhang, Haozhe Xie, and Hongxun Yao. Blur-aware spatio-temporal sparse transformer for video deblurring. In *CVPR*, 2024. 2

[42] Xiaoqiang Zhou, Huaibo Huang, Zilei Wang, and Ran He. Ristra: Recursive image super-resolution transformer with relativistic assessment. *IEEE Transactions on Multimedia*, pages 1–12, 2024. 2